The correlation between X-ray scattering structure factor and shear bands density of a metallic glass and a composite

C. Zhang[a, b, c], T.L. Lee[b, d] J.C. Khong[b, e], J.C. Qiao[c], D. Daisenberger[f], Y. Yao[c], J. Mi[b*]

[a] School of Aeronautics, Northwestern Polytechnical University, Xi'an 710072, P.R. China

[b] School of Engineering & Computer Science, University of Hull, East Yorkshire HU6 7RX, UK

[c] School of Mechanics, Civil Engineering and Architecture, Northwestern Polytechnical University, Xi'an 710072, P.R. China

[d] ISIS Neutron Source, Science and Technology Facilities Council, Rutherford Appleton Laboratory, Harwell Oxford, Didcot OX11 0QX, UK

[e] Department of Medical Physics & Biomedical Engineering, University College London, London WC1E 6BT, UK

[f] Diamond Light Source, Didcot, Oxfordshire OX11 0DE, UK

The corresponding authors: Prof. Jiawei Mi Tel: +44 (0) 1482 465670

E-mail: j.mi@hull.ac.uk

Abstract

The tensile fractured surfaces of ZrTi-based bulk metallic glass and composite samples were studied using synchrotron X-ray total scattering. The scanned areas contain different shear bands densities. The shear bands create localized atomic strains, which in turn cause more ordered atomic structures. Such structural changes were reflected in the scattering structure factor, i.e. the higher the density

of the shear bands, the higher the scattering structure factor. Similar phenomenon was also found in the metallic glass composite.

Keywords: X-ray techniques, Amorphous materials, Metallic composites, shear bands.

1. Introduction

Design and development of novel amorphous alloys and bulk metallic glasses (BMGs) have been the center of research in physics, materials, and engineering communities around the world for many years [1]. Although BMGs have unique physical and chemical properties with high mechanical strengths [2], most of them may have near zero tensile ductility at room temperature [4, 5]. During plastic deformations of BMGs, the nucleation of shear bands and their inhomogeneous propagation play a dominant role in determining their plasticity and ductility [5]. In the past 10-15 years, researchers have used electron or X-ray based imaging and scattering techniques to study the *in-situ* deformations of BMGs and BMG composites (BMGCs) in compressive, tensile, or shearing in order to understand the relationships between the nucleation and propagation of shear bands and the resultant changes in structure at atomic and nanometer scale [5-7]. For example, Shahabi *et al.* found that the shear strain plays important role in triggering the nucleation of more shear bands from a mature shear band, using high energy X-ray beam [8]. Sun *et al.* found that, although BMGs are generally considered as isotropic materials, they could behave anisotropically as the results of manufacturing or deformation [9]. Mattern and Wang *et al.* reported that atom reorientation in the first nearest-neighbor shell resulted in anisotropy near the shear band region [6, 10]. Tensile and bending deformation induced crystallization behaviors were also reported in a Zr-based BMG [11], in an Al-based [12] and a Pb-based metallic glass ribbons [13].

Researchers in Mi's group have conducted a series of in-situ tensile experiments on BMGs [5] and BMGC [7] using electron imaging and synchrotron X-ray diffraction techniques. The general objective of the research is to investigate and understand the evolution of atomic structures, and the nucleation and propagation of shear bands under different stress and strain fields. In this paper, we reported some new findings from the above research, and we found that there is strong correlation between the synchrotron X-ray scattering structure factor and the density of shear bands after deformation, a very interesting phenomenon that applied to both BMGs and BMGC samples.

2. Experimental

Classical ZrTi-based BMG alloy Vit1 (with the normal composition of $Zr_{41.2}Ti_{13.8}Cu_{12.5}Ni_{10}Be_{22.5}$, at. % [14]) and BMGC ($Zr_{39.6}Ti_{33.9}Nb_{7.6}Cu_{6.4}Be_{12.5}$, at. % [15]) were used. The making of the alloy samples and related tensile test are described in details in [7, 16]. Herein, an array of synchrotron X-ray scattering patterns was collected from the fractured samples on the locations where shear bands were present. The detailed experimental and data processing are shown in Supplementary Material.

3. Results and discussion

Fig. 1a and c show the SEM images of the fractured surface of BMG and the BMGC samples, respectively. A 0.4 mm diameter hole at the center of the BMG, and a 0.125 mm radius notch at the edge of the BMGC were drilled as the stress concentrators to initiate shear bands. The framed areas in Fig. 1a and c were enlarged and shown in Fig. 1b and d. The red circles in Fig. 1b and d indicate the locations where the X-ray scatterings were taken. P1 to P6 mark the circles in the BMG sample, while PC1 to PC6 for the BMGC sample. Each circle represents the synchrotron X-ray spot size with a diameter of 70 μm used. The first peak of the structure factors S(Q) for each circle was enlarged and then put together to show their relative difference as illustrated on Fig. 1b and d.

Fig. 2a shows the structure factor S(Q) of measured Vit1 BMG sample marked in Fig. 1c, and Fig. 2b shows the enlarged view of the region near the first peaks. It is very clear that the peak intensity for each location is different and P1 has the highest value, followed by P2 to P6. The first peaks of the S(Q) are reproduced, enlarged and then superimposed onto Fig. 1b. The relative increase in the peak value is also calculated using the lowest one (P6) as the baseline. The first peak intensity diffracted at P1 is increased by 7.4%, and that at P2, P3, P4, P5 is increased by 6.4%, 5.7%, 5.6%, and 3.1%, respectively.

Fig. 1b also shows that the numbers of shear bands at P1 to P6 are gradually decreased. This paper defined the shear band density (SBD) as the ratio of the measured total length of the shear bands within the red circle to the area of that circle. From P1 to P4, the SBD was 33.9, 21.6, 13.3, and 3.0 mm^{-1}, respectively. No visible shear bands were found at P5 and P6 in the SEM image, so zero SBD was used for these two locations. Clearly, the higher the SBD, the higher the first peak of the X-ray scattering structure factor.

Fig. 2c shows all reduced pair distribution function (PDF), G(r), for the 6 locations in the BMG. Fig. 2d shows the enlarged view, and they are all around 3.04 and 3.05 Å. The peak value ($Å^{-2}$) is 3.57, 3.52, 3.49, 3.47, 3.35, and 3.20 for P1 to P6, respectively. The G(r)s show that the P1 has the highest peak value, while P6 has the lowest.

Similar phenomena were found in BMGC sample. Fig. 2e shows the S(Q) for BMGC sample [7] (Fig. 1d), and the enlarged view is shown in Fig. 2f. Clearly, the peak values decrease from PC1 to PC4 (Fig. 1d). From the SEM image, the degree of plastic deformation decrease from PC1 to PC4. As reported in [7], in the region close to PC4, the mark 1 and 2 in the inset of Fig. 3b show

that the shear bands passed the crystalline dendrites and glass matrix. Although it is difficult to count and calculate the SBD because of the two phase tangled together, at PC4, the degree of plastic deformation is the least one among the six circles. Meanwhile, at PC1, PC2 and PC3 the degree of deformation are much higher, resulting in much higher first peaks. The boundary between crystal and glass matrix can be regarded as a mark, which correlate to the degree of plastic deformation. For undeformed region, referring to the top-left corner of Fig. 1d, the boundaries are clear and distinct. In deformed regions, the boundary will become blurred. Because of the clear boarder and image, we can make conclusion that PC4 is the least plastic deformed one among these six circles.

4. Conclusion

In summary, synchrotron X-ray was used to scan the fractured surfaces of BMG and BMGC samples which contain different SBDs. A strong correlation between SBD and the resulting scattering structure factor was found, i.e. the higher the density of the shear bands, the higher the X-ray scattering structure factor. The similar regularity was found in BMGC sample.

CRediT authorship contribution statement

C. Zhang: Methodology, Writing, and Investigation. T.L. Lee: Investigation. J.C. Khong: Software, Formal analysis. J.C. Qiao: review & editing. Y. Yao: review & editing. D. Daisenberger: Methodology, Investigation, Resources. J. Mi: Supervision, Writing - review & editing.

Declaration of Competing Interest

The authors declare that they have no known competing financial interests or personal relationships that could have appeared to influence the work reported in this paper.

Acknowledgements

Dr. C. Zhang would like to thank Shaanxi Natural Science Basic Research Project (2020JQ-114) and the China Scholarship Council for 1 year PhD study at the University of Hull. We acknowledge the synchrotron X-ray beam times awarded by the beamline I15 of Diamond Light Source (experimental No. EE9902-1).

DATA AVAILABILITY

The data that support the findings of this study are available within the article and its supplementary material.

References

[1] Y.H. Liu, G. Wang, R.J. Wang, D.Q. Zhao, M.X. Pan, W.H. Wang, Science 315(5817) (2007) 1385-1388.

[2] A.L. Greer, Nat Mater 14(6) (2015) 542-546.

[3] J.C. Qiao, J.M. Pelletier, J Mater. Sci. Technol. 30(6) (2014) 523-545.

[4] C.A. Schuh, T.C. Hufnagel, U. Ramamurty, Acta Mater. 55(12) (2007) 4067-4109.

[5] Y.J. Huang, J.C. Khong, T. Connolley, J. Mi, Scripta Mater. 69(3) (2013) 207-210.

[6] N. Mattern, J. Bednarcik, S. Pauly, G. Wang, J. Das, J. Eckert, Acta Mater. 57(14) (2009) 4133-4139.

[7] Y. Huang, J. Khong, T. Connolley, J. Mi, Appl. Phys. Lett. 104(3) (2014) 031912.

[8] H.S. Shahabi, S. Scudino, I. Kaban, M. Stoica, B. Escher, S. Menzel, G.B. Vaughan, U. Kühn, J. Eckert, Acta Mater. 111 (2016) 187-193.

[9] Y.H. Sun, A. Concustell, M.A. Carpenter, J.C. Qiao, A.W. Rayment, A.L. Greer, Acta Mater.

112(Supplement C) (2016) 132-140.

[10] G. Wang, N. Mattern, J. Bednarčík, R. Li, B. Zhang, J. Eckert, Acta Mater. 60(6) (2012) 3074-3083.

[11] X. Wang, J. Bednarcik, K. Saksl, H. Franz, Q. Cao, J. Jiang, Appl. Phys. Lett. 91(8) (2007) 081913.

[12] W.H. Jiang, M. Atzmon, Acta Mater. 51(14) (2003) 4095-4105.

[13] A.R. Yavari, K. Georgarakis, J. Antonowicz, M. Stoica, N. Nishiyama, G. Vaughan, M. Chen, M. Pons, Phys. Rev. Lett. 109(8) (2012) 085501.

[14] A. Peker, W.L. Johnson, Appl. Phys. Lett. 63(17) (1993) 2342-2344.

[15] D.C. Hofmann, J.-Y. Suh, A. Wiest, G. Duan, M.-L. Lind, M.D. Demetriou, W.L. Johnson, Nature 451(7182) (2008) 1085-1089.

[16] Y.J. Huang, J.C. Khong, T. Connolley, J. Mi, Int. J Plasticity 60 (2014) 87-100.

Figures

Fig. 1. (a) a SEM image of the fractured Vit1 sample, (b) the enlarged view of the framed area in (a), showing the shear bands, and the red circles, marked P1-P6, representing the locations where synchrotron X-ray diffraction were taken. The first peak of the structure factor, S(Q), for each circle was enlarged and then put together to show the relative difference for different locations. (c) a SEM image of fractured ZrTi-based BMGC sample, (d) the enlarged view of the framed area in (c), showing an obvious plastic deformation, and the red circles, marked PC1-PC6, showing the locations where synchrotron X-ray diffraction were taken. Similarly, the first peak of the structure factor, S(Q), for each circle for BMGC was superimposed on Fig.1d.

Fig. 2. (a) the structure factor, S(Q), for the red circles in Fig. 1b on the BMG sample, (b) the enlarged view for the region near the first peaks of the S(Q) in (a), (c) the corresponding reduced PDFs, G(r), calculated based on the S(Q) in (a), (d) the enlarged view of the first peaks of the G(r) in (c), (e) the structure factor, S(Q) for the ZrTi-based BMGC within the red circles marked in Fig. 1d, and (f) the enlarged view of their first sharp peak.

Fig. 3. (a) the correlation between the first peak of the structure factor, S(Q) and the SBD for the BMG sample, (b) a typical shear band behavior, passing through crystalline dendrites and glassy matrix in the BMGC sample, and the inset showing the enlarged images of the rectangular area.

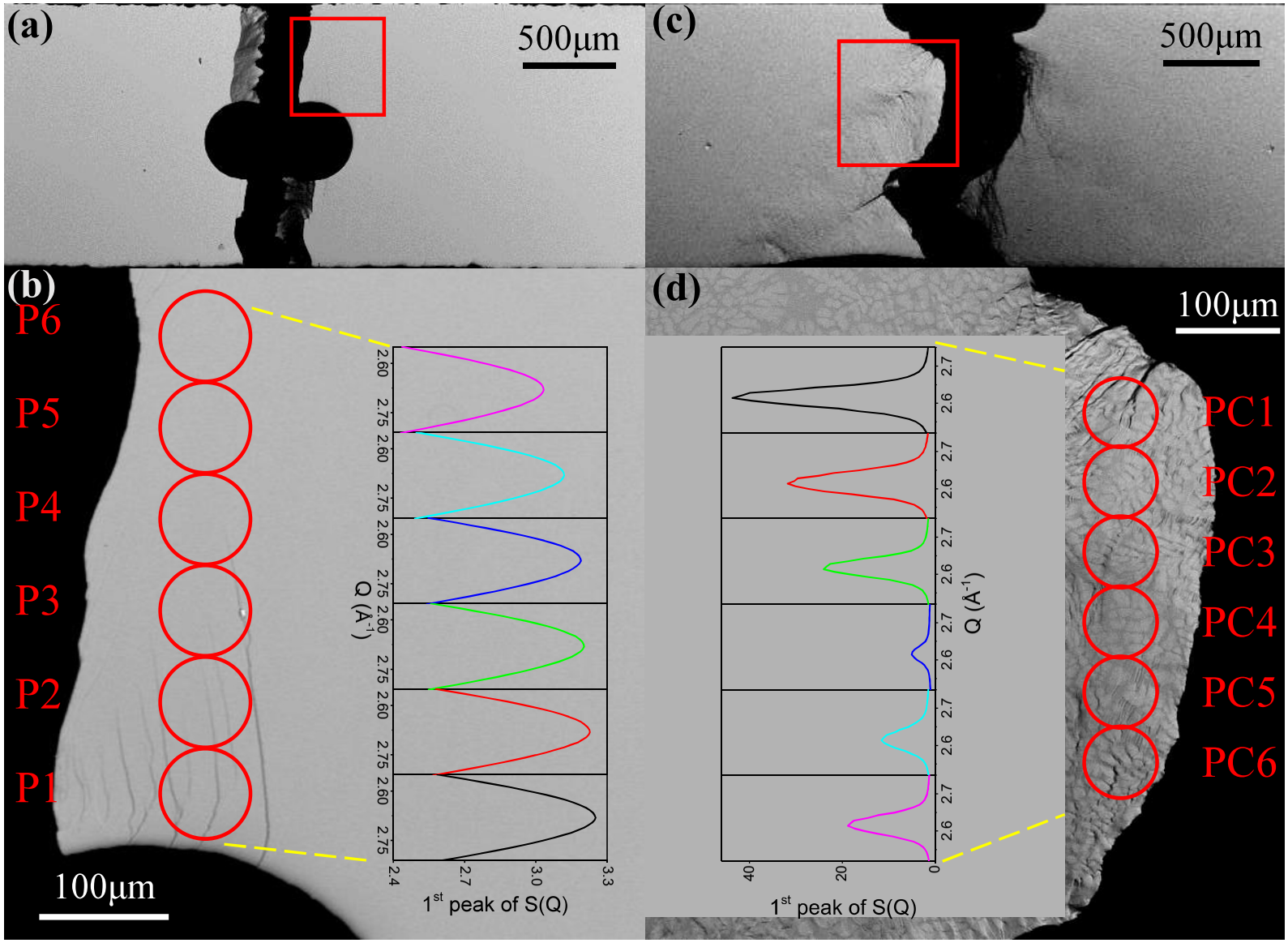

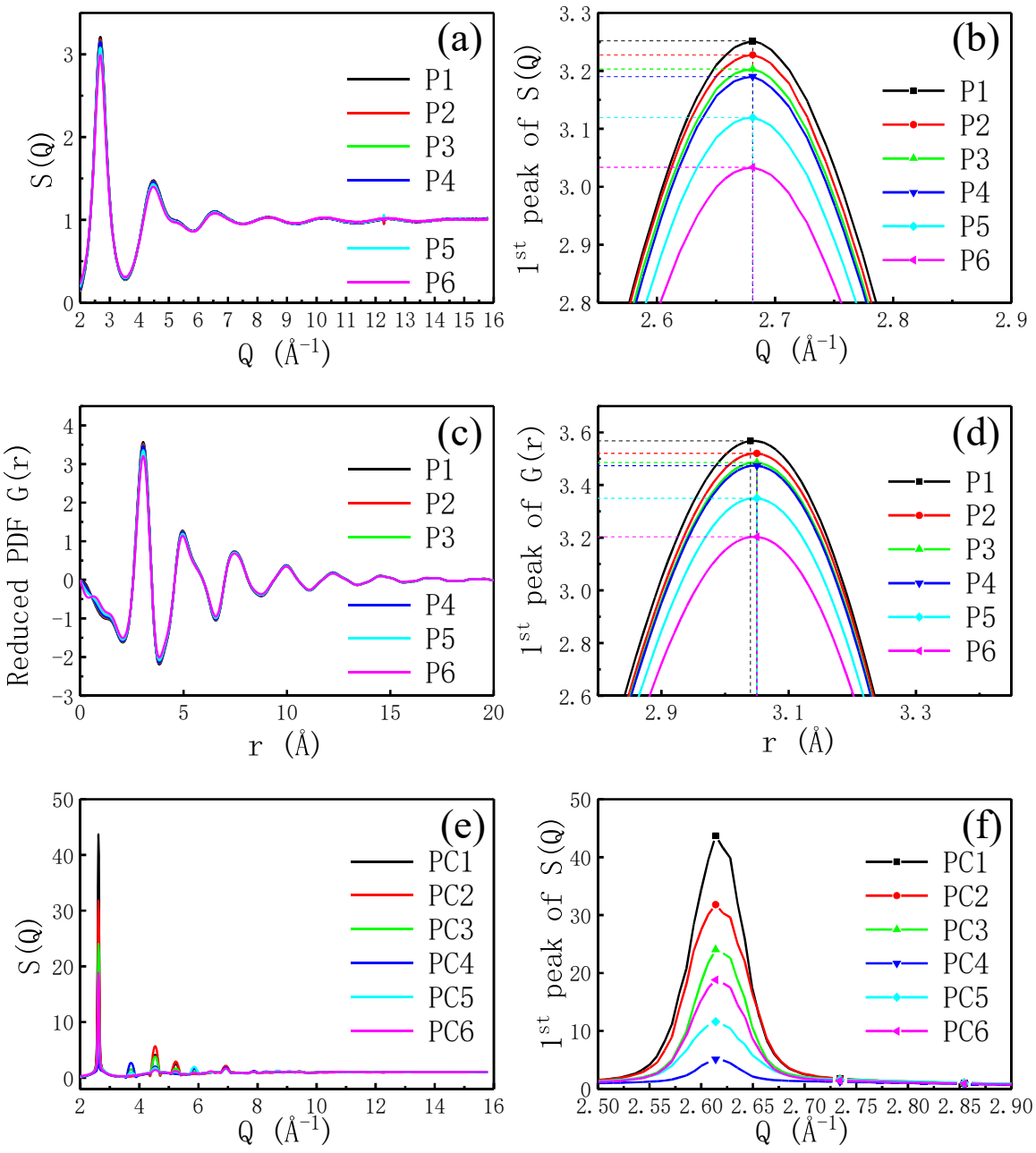

Figure 3

Click here to access/download;Figure;figure3.pptx